

Individually Addressed Quantum Gate Interactions Using Dynamical Decoupling

M.C. Smith^{✉,†}, A.D. Leu^{✉,†}, M.F. Gely^{✉,†} and D.M. Lucas

Clarendon Laboratory, Department of Physics, University of Oxford, Parks Road, Oxford OX1 3PU, United Kingdom



(Received 11 October 2023; revised 19 April 2024; accepted 26 June 2024; published 1 August 2024)

A leading approach to implementing small-scale quantum computers has been to use laser beams, focused to micron spot sizes, to address and entangle trapped ions in a linear crystal. Here we propose a method to implement individually addressed entangling gate interactions, but driven by microwave fields, with a spatial resolution of a few microns, corresponding to 10^{-5} microwave wavelengths. We experimentally demonstrate the ability to suppress the effect of the state-dependent force using a single ion, and find the required interaction introduces $3.7(4) \times 10^{-4}$ error per emulated gate in a single-qubit benchmarking sequence. We model the scheme for a 17-qubit ion crystal, and find that any pair of ions should be addressable with an average crosstalk error of approximately 10^{-5} .

DOI: 10.1103/PRXQuantum.5.030321

Dynamical decoupling (DD) [1–5] is commonly used across many quantum computing platforms to reduce the loss of quantum information caused by decoherence [6–12]. DD aims to suppress the interaction between a quantum system and its environment by imposing a time dependence on the interaction, and averaging out the net effect on the system. This technique is used for enhancing quantum memories [7–12] and reducing errors during logical gate operations [13–16]. Recently, it has been put forth as a promising method to reduce crosstalk from coherent control pulses, for spin [17] and superconducting [18] qubits. In this paper, we extend this idea to selectively decouple qubits within the same register from gate interactions, enabling individual qubit addressing.

We demonstrate this idea using trapped-ion qubits driven by near-field microwaves [14,19–25]. More specifically, we show how DD can enable individually addressed $\hat{\sigma}_x \otimes \hat{\sigma}_x$ gate interactions [14,19–23], addressing a key challenge with microwave-driven trapped ions over the laser-driven alternative. Microwave technology offers attractive features for ion-trap scalability: robustness, cost and size, straightforward amplitude and phase control, and easy integration of waveguides onto surface traps.

However, whilst laser beams can be focused onto individual ions [26], the centimeter wavelength of microwaves requires alternative techniques to address ions confined to the same potential well [27–33]. Individually addressed microwave-driven two-qubit gates have previously been demonstrated using magnetic gradient-induced coupling (MAGIC) [34], however, this technique cannot be used on magnetic field insensitive “clock” qubits and is therefore susceptible to magnetic field fluctuations.

We first show how DD can be used to suppress the effect of the interaction which drives two-qubit gates, the state-dependent force (SDF) [35–37]. The error associated with the suppression of this “state-dependent displacement” (SDD) is measured to be much lower than typical two-qubit gate errors: $3.7(4) \times 10^{-4}$. Secondly, we implement a spatially varying DD phase to selectively suppress or enable the SDD with approximately $1 \mu\text{m}$ spatial resolution, as schematically illustrated in Fig. 1. We extrapolate our results to a larger register of ions, showing how this technique could enable all-to-all connectivity in a chain of ions solely by varying the amplitude of microwave currents in three electrodes.

For this demonstration, a single ion is displaced to different positions to emulate different ions in a chain. Our experiments are carried out at room temperature on a segmented electrode surface “chip” trap characterized in Ref. [38]. The trap features an on-chip microwave (MW) resonator with a single ion trapped $40 \mu\text{m}$ above the chip surface. Our qubit is defined by the hyperfine states $|1\rangle = |F = 4, M_F = 1\rangle$, and $|0\rangle = |F = 3, M_F = 1\rangle$ of the ground-state manifold $4^2\text{S}_{1/2}$ of $^{43}\text{Ca}^+$, which form a clock qubit at our static magnetic field strength of 28.8 mT . These states are connected by a magnetic dipole transition with

*Contact author: molly.smith@physics.ox.ac.uk

†These authors contributed equally.

Published by the American Physical Society under the terms of the [Creative Commons Attribution 4.0 International license](#). Further distribution of this work must maintain attribution to the author(s) and the published article’s title, journal citation, and DOI.

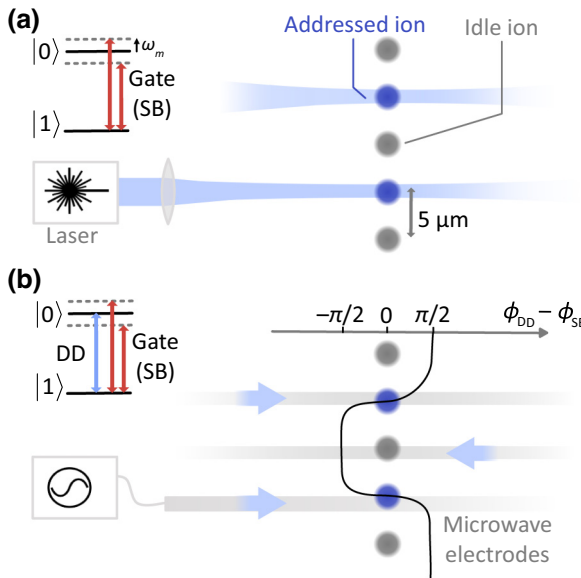


FIG. 1. Two-qubit gate addressing through spatially varying dynamical decoupling. (a) A laser is commonly used to address ions by focusing beams to small spot sizes [26]. To drive the two-qubit gate interaction—state-dependent force (SDF)—two sideband (SB) laser tones are applied, symmetrically detuned from the qubit frequency by the motional frequency ω_m . (b) An SDF can also be driven using microwave currents, tuned to SB frequencies, and injected through electrodes (light gray) passing under the ions. Due to the long wavelength of microwaves, this force will affect all ions trapped within the same potential well. Our proposed method for targeting a single ion requires an additional dynamical decoupling tone, which drives the qubit resonantly. By spatially varying the phase difference between DD and SB drives—through interference of the field generated by the different electrodes—the effect of the SDF is either enabled (DD and SB in phase) or suppressed (DD and SB in quadrature).

frequency splitting $\omega_q = 2\pi \times 3.1$ GHz. To drive this transition, we use near-field radiation generated by the currents propagating in the MW resonator. The field gradient is used to generate the SDF enabling two-qubit gates.

An SDF is generated by driving the red and blue motional sidebands of the qubit transition at frequencies $\omega_q \pm \omega_m$ (see Sec. S1 within the Supplemental Material [39]) where ω_m corresponds to the frequency of one of the motional modes of the ion—here we use the in-plane radial mode ($\omega_m = 2\pi \times 5.77$ MHz). The SDF displaces the state of this mode in position-momentum phase space where the sign of the displacement depends on the qubit state [40]. By slightly detuning from the red and blue sidebands, the motion describes loops in phase space—the central mechanism of Mølmer-Sørensen (MS) two-qubit gates [35–37]—but we will mostly focus on the resonant case for simplicity, and without loss of applicability to the detuned case. Under a rotating-wave approximation and ignoring negligible off-resonant carrier driving, the SDF

is described by the Hamiltonian (see Sec. S1 within the Supplemental Material [39])

$$\hat{H}_{\text{SDF}} = \frac{\hbar}{2} \Omega_{\text{SB}} \hat{\sigma}_x (\hat{a} + \hat{a}^\dagger), \quad (1)$$

here written in the interaction frame with respect to the qubit and motion, where Ω_{SB} is the sideband interaction strength, proportional to the gradient of the field driving the ion. Rewritten as

$$\hat{H}_{\text{SDF}} = \frac{\hbar}{2} \Omega_{\text{SB}} |+\rangle \langle +| (\hat{a} + \hat{a}^\dagger) - \frac{\hbar}{2} \Omega_{\text{SB}} |-\rangle \langle -| (\hat{a} + \hat{a}^\dagger) \quad (2)$$

the state-dependent force is made explicit: the motion experiences a force, which is positive if the qubit is in state $|+\rangle = (|0\rangle + |1\rangle)/\sqrt{2}$ and negative if the qubit state is $|-\rangle = (|0\rangle - |1\rangle)/\sqrt{2}$.

We propose to selectively suppress the state-dependent displacement driven by the SDF through the choice of the phase of an additional dynamical decoupling tone driving the qubit transition. For the MW electrode geometry used in this experiment, the dynamical decoupling drive phase changes with ion position, localizing the effect to a chosen region of space. The DD tone drives the interaction

$$\hat{H}_{\text{DD}} = \frac{\hbar}{2} \Omega_{\text{DD}} e^{i\phi_{\text{DD}}} \hat{\sigma}_+ + \text{h.c.}, \quad (3)$$

where $\hat{\sigma}_+ = |1\rangle \langle 0|$, Ω_{DD} is the strength of the DD drive, and the phase ϕ_{DD} depends on the ion position and the phase of the injected microwave current. Note that if the DD and SDF are in phase, $\phi_{\text{DD}} = k\pi$ ($k \in \mathbb{Z}$), the Hamiltonians commute, $[\hat{H}_{\text{SDF}}, \hat{H}_{\text{DD}}] = 0$, and the dynamical decoupling does not alter the SDF dynamics. Whilst this has already been demonstrated in two-qubit gates [14], here we also make use of the in-quadrature case.

When the DD and SDF are in quadrature $\phi_{\text{DD}} = \pi/2 + k\pi$, DD driving can suppress the effect of the qubit-motion interaction. The DD tone will drive Rabi oscillations between the states on which the SDF depends $|+\rangle \leftrightarrow |-\rangle$, and, if $\Omega_{\text{DD}} \gg \Omega_{\text{SB}}$, the rapid changes of SDF direction will stop the motion from gaining significant amplitude in phase space. We propose to combine this technique with a microwave electrode geometry that enforces $\phi_{\text{DD}} = k\pi$ for ion positions where the SDF is desired, and $\phi_{\text{DD}} = \pi/2 + k\pi$ for ion positions where the SDF is undesired. First, however, we experimentally demonstrate SDD suppression at a fixed ion position.

Choosing to resonantly drive the sidebands, and subsequently measuring the qubit state, provides a straightforward measurement of the SDD and its suppression. We first demonstrate the effect of the SDF with no DD driving, as shown in Fig. 2(a). Each experimental cycle starts by preparing the state $|0\rangle |0_m\rangle$, where $|0_m\rangle$ designates

the motional ground state through microwave-enhanced optical pumping [21] and Raman-laser driven sideband cooling [38]. A small thermal population does remain in the motional mode (see Sec. S3 within the Supplemental Material [39]), which is included in all our simulations, but omitted here for simplicity. After driving the motional sidebands for a duration t , the initial state

$$|0\rangle |0_m\rangle = \frac{1}{\sqrt{2}} (|+\rangle + |-\rangle) |0_m\rangle \quad (4)$$

will evolve under the SDF to

$$\begin{aligned} |\psi\rangle &= \frac{1}{\sqrt{2}} (|+\rangle |+\alpha\rangle + |-\rangle |-\alpha\rangle) \\ &= \frac{1}{2} |0\rangle (|\alpha\rangle + |-\alpha\rangle) + \frac{1}{2} |1\rangle (|\alpha\rangle - |-\alpha\rangle), \end{aligned} \quad (5)$$

schematically shown in Fig. 2(a), where $|\pm\alpha\rangle$ designates a coherent state with amplitude $\pm\alpha = \pm\Omega_{\text{SB}}t/2$. The probability $P_{|0\rangle}$ of measuring the initial qubit state $|0\rangle$ then decays to 1/2 as α increases, following

$$\begin{aligned} P_{|0\rangle} &= \frac{1}{4} (\langle\alpha| + \langle-\alpha|) \mathbb{1} (|\alpha\rangle + |-\alpha\rangle) \\ &= \frac{1}{2} \left(1 + e^{-2|\alpha|^2} \right), \end{aligned} \quad (6)$$

providing a measurement of the SDD (and later its suppression). For simplicity, we describe the state $|\psi\rangle$ as pure, but in addition to initial thermal population, coherence is degraded by the motional mode heating rate of approximately 370 quanta/s, comparable to the sideband interaction strength $\Omega_{\text{SB}}/2\pi = 380$ Hz. Loss of coherence increases the rate at which $P_{|0\rangle}$ decays, but the physical intuition presented here remains valid, and the measurement still provides a measurement of α once the independently measured heating rate and initial motional mode occupation are considered (see Sec. S3 within the Supplemental Material [39]). The qubit state is read out by transferring $|0\rangle$ to the “dark” $3^2D_{5/2}$ manifold and measuring the probability of the ion fluorescing [41]. A measurement of the decay of $P_{|0\rangle}$ to 0.5, as a consequence of the SDF, is shown in Fig. 2(b).

Driving the system at both DD and sideband frequencies, and varying their relative phases, allows us to suppress the SDD. To demonstrate this, the qubit state is measured after a pulse duration which, at most, will reduce $P_{|0\rangle}$ to 0.6 when the DD drive commutes with the SDF. To ensure that Rabi oscillations induced by DD driving do not have an impact on the final qubit state (independently of the SDF), we switch the phase of the DD drive in a Walsh-3 pattern [42] (see Sec. S4 within the Supplemental Material [39]). The resulting data, shown in Fig. 2(c), clearly shows that the SDD can be either undisturbed or suppressed by selecting DD phases 0 or $\pi/2$, respectively. For

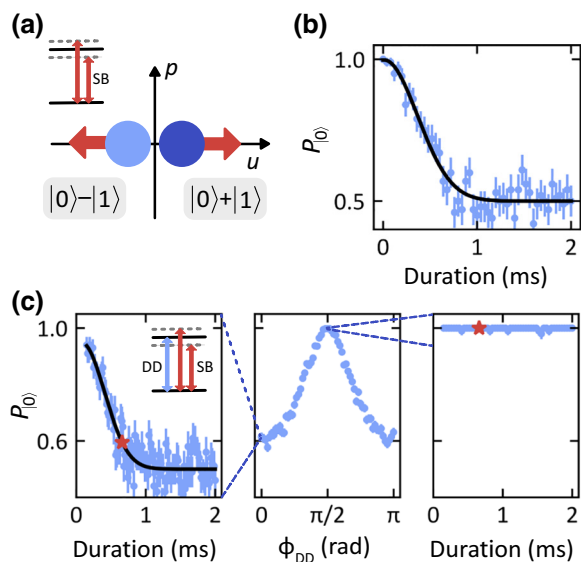


FIG. 2. Suppressing the effect of the state-dependent force through dynamical decoupling. (a) Position-momentum (u - p) diagram illustrating the effect of the state-dependent force (SDF) on the ion’s motional state. Starting with qubit state $|0\rangle$, a measurement in the qubit basis ($|0\rangle$, $|1\rangle$), would show the qubit evolving from state $|0\rangle$ to $(|0\rangle \pm |1\rangle)/\sqrt{2}$. (b) Measured (blue) and fitted (black) probability $P_{|0\rangle}$ of measuring the initial state $|0\rangle$ after driving an SDF using two microwave sideband tones. (c) To inhibit motional entanglement, a dynamical decoupling tone drives the qubit with a variable phase ϕ_{DD} (relative to the average phase of the two sidebands). We measure $P_{|0\rangle}$ for a fixed pulse duration (red star), such that suppression of the state-dependent displacement corresponds to $P_{|0\rangle} > 0.6$. Measurements were taken at a fixed ion position (null of the rf trapping field). The SDD is unaffected ($P_{|0\rangle} \approx 0.6$) or suppressed ($P_{|0\rangle} \approx 1$) for $\phi_{\text{DD}} = 0$ and $\phi_{\text{DD}} = \pi/2$, respectively. All error bars indicate 68% confidence intervals.

this demonstration, we fix the DD drive power injected into the trap such that the DD drive amplitude $\Omega_{\text{DD}} = 60 \Omega_{\text{SB}}$, which fulfills the requirement for suppression $\Omega_{\text{DD}} \gg \Omega_{\text{SB}}$ (see Sec. S4 within the Supplemental Material [39]). Note that the microwave power of the dynamical decoupling tone, required to obtain $\Omega_{\text{DD}} = 60 \Omega_{\text{SB}}$, is 2 orders of magnitude smaller than the power injected at sideband frequencies due to the small effective Lamb-Dicke parameter $\eta = 1.25 \times 10^{-3}$ (see definition in Sec. S1 within the Supplemental Material [39]).

To use this technique to address individual ions, the phase difference between the DD driving and SDF at different ion positions must vary—in our system this arises from the microwave electrode geometry, schematically shown in Fig. 3(a). The ion is driven by near-field radiation generated by MW currents flowing in a U-shaped electrode (see Ref. [38] for more details). Currents propagate in opposite directions on each side of the ion (approximately π radians out of phase), leading to destructive interference

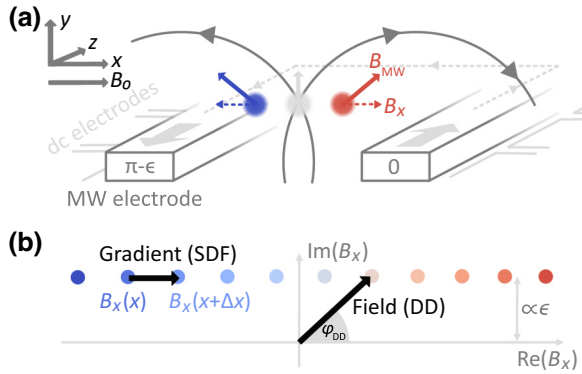


FIG. 3. Surface-trap design giving a spatially varying phase. (a) Schematic of our surface trap. Two microwave electrodes produce interfering microwave fields. These fields combine to produce B_{MW} (solid arrow). The component B_x of this field (dashed arrow)—in the direction of the quantisation axis, defined by a static field B_0 —drives qubit transitions. The two microwave electrodes are connected 750 μm away from the ion (gray dashed line) and their currents are approximately π radians out of phase (with a small phase offset ϵ). (b) B_x phasor in the complex plane (dots) where the imaginary axis has been magnified $\times 20$. Neighboring dots correspond to ion positions 2 μm apart in the x direction. As the ion is moved along the x axis, the phase of the microwave field, dictating the phase ϕ_{DD} , changes by approximately π radians. The phase of the field gradient, however, remains constant and thus so does that of the state-dependent force. The change in phase of the field is used to obtain suppression of the state-dependent displacement away from the symmetry point of the microwave field.

of the magnetic field component B_x aligned with the quantisation axis B_0 [see Fig. 3(a) for the coordinate system], which is the component of the field that couples to our “ π -polarized” qubit transition. The interference leads to a change in the phase of B_x as a function of x , since the field switches from being dominated by the field of one electrode to the other. This is illustrated by plotting B_x in the complex plane, see Fig. 3(b). The phase of the gradient of the B field however, which determines the phase of the SDF (see Sec. S1 within the Supplemental Material [39]), stays constant as the ion is moved across the trap.

The phase of the DD drive therefore changes with position, undergoing a phase shift of approximately π radians, whereas the phase of the SDF remains constant. As a result, the DD and SDF can be in phase at the x position of the field minimum whilst being approximately $\pm\pi/2$ out of phase away from it. An experimental verification of this is shown in Fig. 4(a). The change in DD drive phase is measured by preparing (and measuring) the $|+\rangle$ state at $x = 0$ before (and after) displacing the ion to position x , where it is subject to a MW pulse with varying phase ϕ_p . When averaged over multiple random pulse amplitudes, sweeping the phase ϕ_p to maximize the probability of measuring $|+\rangle$ at the end of the sequence constitutes

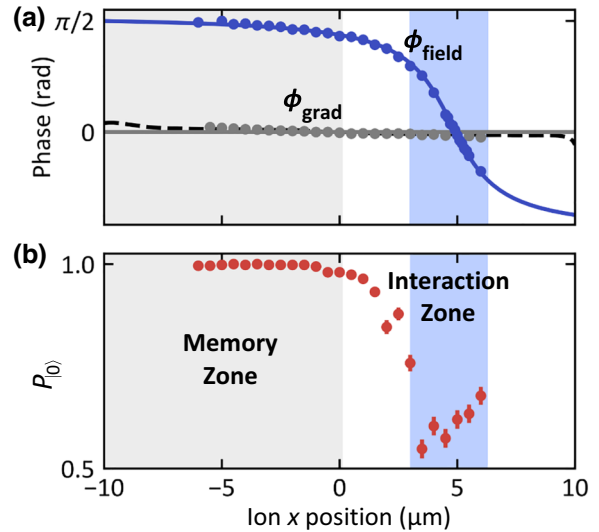


FIG. 4. Spatially selective ion-motion interaction. (a) Measured phase of the microwave field (blue dots) and its gradient (gray dots), with fits (solid lines) to a Biot-Savart model of the trap (see Sec. S2 within the Supplemental Material [39]). Here $x = 0$ corresponds to the null of the rf trapping field. The two shaded regions correspond to the microwave field and its gradient being $\pi/2$ radians out of phase (gray) or in phase (blue). The gradient of the microwave field features a slight change in its phase caused by a tilt in the direction of the ion's harmonic motion, consistent with simulated values (black dashed line). (b) After preparing state $|0\rangle$ at position $x = 0$, the ion is displaced to position x , subjected to SB and DD driving, and returned to position $x = 0$ where we measure the probability $P_{|0\rangle}$ of finding the qubit in its initial state. The phase of the DD drive injected into the trap is kept constant, but the MW electrode geometry offsets the DD phase at the ion position as shown in (a). This leads to a memory zone (gray) where the state-dependent displacement is suppressed and an interaction zone (blue), where it is not. Here, the interaction zone is defined as where $P_{|0\rangle}$ is below 0.75. All error bars indicate 68% confidence intervals.

a measurement of the field’s position-dependent phase shift (see Sec. S2 within the Supplemental Material [39]). The phase of the SDF is measured relative to the DD by maximizing $P_{|0\rangle}$ in a DD phase scan, as described in Fig. 2(c), for different ion positions. Ion displacement is achieved by varying the voltage delivered to the trap dc electrodes following an analytical model of the trapping field (see Ref. [43]). Notably, we measure a slight change in the SDF phase—rather than the desired constant phase—which arises from a change in the direction of the ion’s harmonic motion, which samples the microwave gradient in the y direction. This results from the limited control offered by our dc trap electrode geometry when displacing the ion from the trap rf null (see Sec. S3 within the Supplemental Material [39]).

The spatial variation in MW phase will “enable” the SDD for an ion displaced by $x \approx 5 \mu\text{m}$ from the trap rf null but the SDD will be increasingly suppressed by the

DD drive when the ion is displaced out of this “interaction zone,” creating a much broader “memory zone.” Experimental verification of this is carried out as in Fig. 2(c), but where the phase of the DD tone injected in the trap is kept constant, and the ion position is varied instead. To disentangle the change in relative phase of the DD from changes in motional mode properties, we vary the pulse duration and sideband frequency with position. (We refer here to changes in motional mode frequency, thermal occupation, or heating rate, as well as the change in direction of motion, which are measured and presented in Sec. S3 within the Supplemental Material [39] but which would not be present in applications of this technique where ions are not displaced, see Fig. 5.) The pulse duration is chosen such that, starting in state $|0\rangle$ and in the absence of DD driving, the SDF causes a decay of $P_{|0\rangle}$ to 0.51. The measurements, shown in Fig. 4(b), reveal the variation in the effect of the state-dependent force as an ion is moved across the surface trap, and the resulting “interaction” and “memory” zones.

This technique, extended to two interaction zones, could be used to drive two-qubit gates between arbitrary pairs of ions arranged in a chain, without resorting to ion shuttling. We propose a different trap design, which would facilitate this, shown in Fig. 5(a), where the chain of ions is now perpendicular to the microwave electrodes. This could be accomplished by using a multilayer surface trap [44], possibly where buried microwave electrodes emerge under the ions [45]. Here the additional interaction zone is enabled by a third microwave electrode creating a second DD phase flip (at a different position to the first). The three electrodes are assumed to be fed by independent microwave currents, where the central MW current is close to π radians out of phase with the other two. For our simulations, we set a phase difference $(\pi - \epsilon)$ radians, where $\epsilon = 3 \times 10^{-5}$ (based on a typical figure for the demonstrated accuracy in MW phase control [46]). The phase offset ϵ sets the “steepness” of the phase gradient, and therefore the width of the interaction zone. The positions of the two phase flips, and corresponding interaction zones, can be set through the amplitudes of the DD currents through each electrode. The SDF strength at both zones can also be set independently by varying the SB currents through each electrode.

We simulate the expected crosstalk when performing two-qubit gates between all pairs in a chain of 17 ions, with a uniform ion spacing of 5 μm and an ion height of 40 μm . We assume that the leading source of crosstalk would be imperfect control over the spatial variation in DD phase, i.e., $\phi_{\text{DD}} - \phi_{\text{SB}} \neq \pm\pi/2$ and neglect other sources of crosstalk (see Sec. S5 within the Supplemental Material [39]). Crosstalk here measures the impurity of the partial trace of nonaddressed ions after a gate. In Fig. 5(b), we consider the worst affected nonaddressed ion for a given pair of addressed ions and so, since we are not showing the average crosstalk across the chain,

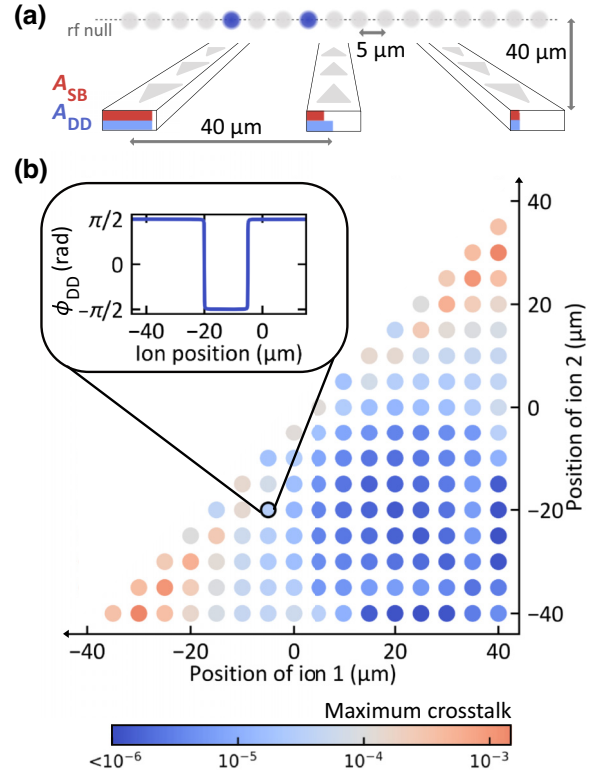


FIG. 5. Simulated surface trap with three microwave electrodes. (a) Schematic of the proposed trap design using three microwave electrodes. The ion-chain lies perpendicular to the microwave electrodes. A pair of ions (dark blue) have been selected to demonstrate this scheme. Bar plots on each electrode show the required sideband (red) and dynamical decoupling (blue) amplitudes to address this ion pair. (b) Maximum crosstalk—due to imperfect suppression of the effect of the state-dependent force (SDF) at the nonaddressed ions—when driving an SDF on both ions in a pair simultaneously. The DD phase (corresponding to the microwave field phase) is shown for the ion pair selected in (a).

we refer to this as “maximum crosstalk.” Alternatively, if we consider the mean crosstalk across the chain, we find a crosstalk error of $1.04(9) \times 10^{-5}$ (averaging over all addressed ion pairs). This shows that all-to-all connectivity is possible with crosstalk error rates (due to imperfect SDD suppression at the nonaddressed ions) far below typical error-correction thresholds. Errors are lowest between the electrodes—the natural location for creating field interference—but increase as ion pairs are moved further out. Adding more microwave electrodes or bringing the phase difference between currents closer to π radians reduces these errors and would enable even larger registers of ions.

For this design, we have considered the chain of ions to be perpendicular to the MW electrodes, for an implementation of gates on axial motional modes. However, changing the angle between the ion chain and MW electrodes would also enable the use of radial motional modes.

As the ion chain gets closer to being parallel with the MW electrodes, the radial MW gradient increases, and narrower interaction zones are required. Alternatively, one could use separate electrodes for dynamical decoupling (perpendicular to the ion chain) and sideband driving (parallel to the ion chain, maximizing the radial MW gradient). Neither electrode direction should, however, be perpendicular to the quantization axis.

In practice, the combination of low ion height and long chains is likely to exacerbate issues of anomalous motional heating [47] and limited ion lifetime [48]. To mitigate these, cryogenic operation will probably be required [38]. To further limit the impact of heating, the use of out-of-phase motional modes (rather than center-of-mass modes) should be favored [47]. If these issues are too severe, mode frequencies can be raised (reducing inter-ion spacing for axial modes), or the ion height can be increased [47]. However, such solutions would require finer microwave phase control (more specifically control over ϵ) to maintain low crosstalk, and would reduce gate speeds. Other issues with long chains are shared with previous implementations, for example, motional frequency crowding, requiring more complex amplitude and phase shaping [49,50], and the reduction in gate speed resulting from the increase in effective mode mass. Gate fidelities will also be affected by drifts in the ion's position [51], and we expect that active stabilization will be required to combat this issue, as discussed in Sec. S5 within the Supplemental Material [39]. These considerations will ultimately determine the optimal number of ions to use in a chain, and will be influenced by progress in reducing anomalous heating, stabilizing the ion's position and controlling the relative microwave phase between on-chip electrodes.

We measure to what extent the theoretical crosstalk would be dominated by other effects in our system by driving a “suppressed” Mølmer-Sørensen (MS) interaction in a randomized-benchmarking-type measurement [52] (see Sec. S6 within the Supplemental Material [39]). We detune the sidebands by $2\pi \times 770$ Hz in a 1.30 ms pulse to emulate—on a single-ion radial mode—a 1-loop MS gate for a Rabi frequency of $\Omega_{\text{SB}} = 2\pi \times 380$ Hz, and apply a DD drive aiming to suppress the effect of this interaction. Due to the large heating rate of this mode, an unsuppressed motional interaction is expected to completely decohere the qubit. The “suppressed MS gate” is applied after every Clifford gate of a single-qubit randomized-benchmarking sequence. We first run a test measurement with $\phi_{\text{DD}} = 0$, to verify the effectiveness of the RB sequences in revealing motional interaction. As expected, we find that the error signal rises to its maximum value (0.5), indicating that the MS pulses lead to a complete loss of coherence as a result of motional interaction. We then change the DD phase to $\phi_{\text{DD}} = \pi/2$ to suppress the effect of the MS interaction, and obtain an error per “suppressed MS gate” of $3.7(4) \times 10^{-4}$, shown in Fig. 6. DD driving alone produces

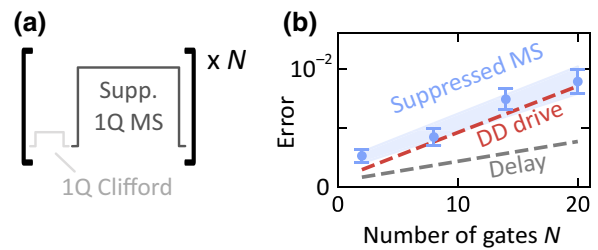


FIG. 6. Single-qubit randomized benchmarking of the suppression error during a gate. (a) The residual error after suppressing the SDD during a gate is experimentally estimated by embedding Mølmer-Sørensen (MS) gate pulses, applied to a single ion and suppressed through a DD drive ($\phi_{\text{car}} = \pi/2$), in a single-qubit randomized benchmarking (RB) sequence. (b) An error of $3.7(4) \times 10^{-4}$ is demonstrated (blue), indistinguishable from the error induced by DD driving alone (red dashed line) indicating a complete suppression of the effect of the ion-motion interaction. The DD driving error is partially accounted for by laser leakage and qubit decoherence, measured by replacing the MS pulse by a delay of equal duration (gray dashed line) (see Sec. S6 within the Supplemental Material [39]). Error bars indicate 68% confidence intervals of the measurements and the shaded region indicates a 68% confidence interval of the fit.

the same error, $4.0(6) \times 10^{-4}$, suggesting that residual qubit-motion entanglement is negligible compared to this measured error, which is probably of technical origin. This error is still far below typical error-correcting thresholds, suggesting the strong potential for scaling to multi-ion registers. Finally, we measure the error arising if the MS pulse is replaced by an equally long time delay, revealing that about half of the error, $1.7(2) \times 10^{-4}$, is not related to the microwave driving at all.

In conclusion, we have demonstrated a method to perform individually addressed gate interactions with a spatial resolution finer than typical inter-ion spacings. To do so, we make use of (1) state-dependent displacement suppression using dynamical decoupling, and (2) a microwave electrode geometry which generates interference, bringing the DD drive in and out of phase with the state-dependent force. Building upon these concepts, we have proposed a surface-trap design to create and move two interaction zones over a chain of ions. We predict that this will enable all-to-all connectivity between ions with crosstalk levels far below error-correction thresholds. The crosstalk error of $3.7(4) \times 10^{-4}$, emulated in a single-ion benchmarking experiment, supports this prediction.

This technique could make microwave-driven logic a more practical approach to constructing a large-scale universal quantum processor by reducing its reliance on shuttling ions. Once two-qubit gates implemented on a chain of ions become limited by the length of the chain, for example, due to multimode effects [53,54], one could then rely on shuttling between different logical zones [55] or optical networking [56]. Additionally, this method is

compatible with pulse amplitude and phase-shaping techniques commonly employed to mitigate errors associated with the many motional modes present in long ion chains [49,50], so long as the amplitude ratio and phase difference between the DD and SDF drives are kept constant. The proposed microwave electrode geometry can also generate a microwave amplitude gradient enabling addressed single-qubit gates with very low ($<10^{-4}$) errors [33], which, combined with the method for addressed two-qubit gates presented in this report, forms a universal, addressed, gate set. Finally, the technique could find applications in a “quantum CCD” architecture [55], where entire registers of ions could be dynamically decoupled from gate interactions to mitigate crosstalk problems.

ACKNOWLEDGMENTS

This work was supported by the U.S. Army Research Office (Ref. W911NF-18-1-0340) and the U.K. EPSRC Quantum Computing and Simulation Hub. M.C.S. acknowledges support from Balliol College. A.D.L. acknowledges support from Oxford Ionics Ltd. M.F.G. acknowledges support from the Netherlands Organization for Scientific Research (NWO) through a Rubicon Grant.

M.C.S., A.D.L., and M.F.G. contributed equally to this work. A.D.L. carried out simulations of the scheme for this experiment and larger ion registers. M.C.S. and M.F.G. acquired and analysed the data. M.C.S. and M.F.G. wrote the manuscript with contributions from all authors. M.C.S., A.D.L., and M.F.G. upgraded and maintained the experiment. D.M.L. and M.F.G. supervised the project.

- [1] L. Viola and S. Lloyd, Dynamical suppression of decoherence in two-state quantum systems, *Phys. Rev. A* **58**, 2733 (1998).
- [2] L. Viola, E. Knill, and S. Lloyd, Dynamical decoupling of open quantum systems, *Phys. Rev. Lett.* **82**, 2417 (1999).
- [3] E. L. Hahn, Spin echoes, *Phys. Rev.* **80**, 580 (1950).
- [4] H. Y. Carr and E. M. Purcell, Effects of diffusion on free precession in nuclear magnetic resonance experiments, *Phys. Rev.* **94**, 630 (1954).
- [5] S. Meiboom and D. Gill, Modified spin-echo method for measuring nuclear relaxation times, *Rev. Sci. Instrum.* **29**, 688 (1958).
- [6] D. Suter and G. A. Álvarez, Colloquium: Protecting quantum information against environmental noise, *Rev. Mod. Phys.* **88**, 041001 (2016).
- [7] N. Ezzell, B. Pokharel, L. Tewala, G. Quiroz, and D. A. Lidar, Dynamical decoupling for superconducting qubits: A performance survey, *Phys. Rev. Appl.* **20**, 064027 (2023).
- [8] M. J. Biercuk, H. Uys, A. P. VanDevender, N. Shiga, W. M. Itano, and J. J. Bollinger, Optimized dynamical decoupling in a model quantum memory, *Nature* **458**, 996 (2009).
- [9] S. Damodarakurup, M. Lucamarini, G. Di Giuseppe, D. Vitali, and P. Tombesi, Experimental inhibition of decoherence on flying qubits via “bang-bang” control, *Phys. Rev. Lett.* **103**, 040502 (2009).
- [10] J. Du, X. Rong, N. Zhao, Y. Wang, J. Yang, and R. B. Liu, Preserving electron spin coherence in solids by optimal dynamical decoupling, *Nature* **461**, 1265 (2009).
- [11] E. R. Jenista, A. M. Stokes, R. T. Branca, and W. S. Warren, Optimized, unequal pulse spacing in multiple echo sequences improves refocusing in magnetic resonance, *J. Chem. Phys.* **131**, 204510 (2009).
- [12] Z.-H. Wang, G. de Lange, D. Ristè, R. Hanson, and V. V. Dobrovitski, Comparison of dynamical decoupling protocols for a nitrogen-vacancy center in diamond, *Phys. Rev. B* **85**, 155204 (2012).
- [13] T. R. Tan, J. P. Gaebler, R. Bowler, Y. Lin, J. D. Jost, D. Leibfried, and D. J. Wineland, Demonstration of a dressed-state phase gate for trapped ions, *Phys. Rev. Lett.* **110**, 263002 (2013).
- [14] T. P. Harty, M. A. Sepiol, D. T. C. Allcock, C. J. Ballance, J. E. Tarlton, and D. M. Lucas, High-fidelity trapped-ion quantum logic using near-field microwaves, *Phys. Rev. Lett.* **117**, 140501 (2016).
- [15] T. Manovitz, A. Rotem, R. Shaniv, I. Cohen, Y. Shapira, N. Akerman, A. Retzker, and R. Ozeri, Fast dynamical decoupling of the Mølmer-Sørensen entangling gate, *Phys. Rev. Lett.* **119**, 220505 (2017).
- [16] P. Barthel, P. H. Huber, J. Casanova, I. Arrazola, D. Niroomand, T. Sriarunothai, M. B. Plenio, and C. Wunderlich, Robust two-qubit gates using pulsed dynamical decoupling, *New J. Phys.* **25**, 063023 (2023).
- [17] D. Buterakos, R. E. Throckmorton, and S. Das Sarma, Crosstalk error correction through dynamical decoupling of single-qubit gates in capacitively coupled singlet-triplet semiconductor spin qubits, *Phys. Rev. B* **97**, 045431 (2018).
- [18] V. Tripathi, H. Chen, M. Khezri, K.-W. Yip, E. Levenson-Falk, and D. A. Lidar, Suppression of crosstalk in superconducting qubits using dynamical decoupling, *Phys. Rev. Appl.* **18**, 024068 (2022).
- [19] C. Ospelkaus, C. E. Langer, J. M. Amini, K. R. Brown, D. Leibfried, and D. J. Wineland, Trapped-ion quantum logic gates based on oscillating magnetic fields, *Phys. Rev. Lett.* **101**, 090502 (2008).
- [20] C. Ospelkaus, U. Warring, Y. Colombe, K. Brown, J. Amini, D. Leibfried, and D. J. Wineland, Microwave quantum logic gates for trapped ions, *Nature* **476**, 181 (2011).
- [21] T. P. Harty, D. T. C. Allcock, C. J. Ballance, L. Guidoni, H. A. Janacek, N. M. Linke, D. N. Stacey, and D. M. Lucas, High-fidelity preparation, gates, memory, and readout of a trapped-ion quantum bit, *Phys. Rev. Lett.* **113**, 220501 (2014).
- [22] G. Zarantonello, H. Hahn, J. Morgner, M. Schulte, A. Bautista-Salvador, R. F. Werner, K. Hammerer, and C. Ospelkaus, Robust and resource-efficient microwave near-field entangling ${}^9\text{Be}^+$ gate, *Phys. Rev. Lett.* **123**, 260503 (2019).
- [23] H. Hahn, G. Zarantonello, M. Schulte, A. Bautista-Salvador, K. Hammerer, and C. Ospelkaus, Integrated ${}^9\text{Be}^+$ multi-qubit gate device for the ion-trap quantum computer, *npj Quantum Inf.* **5**, 2 (2019).

- [24] S. Weidt, J. Randall, S. C. Webster, K. Lake, A. E. Webb, I. Cohen, T. Navickas, B. Lekitsch, A. Retzker, and W. K. Hensinger, Trapped-ion quantum logic with global radiation fields, *Phys. Rev. Lett.* **117**, 220501 (2016).
- [25] R. Srinivas, S. C. Burd, H. M. Knaack, R. T. Sutherland, A. Kwiatkowski, S. Glancy, E. Knill, D. J. Wineland, D. Leibfried, A. C. Wilson, D. T. C. Allcock, and D. H. Slichter, High-fidelity laser-free universal control of trapped ion qubits, *Nature* **597**, 209 (2021).
- [26] H. C. Nägerl, D. Leibfried, H. Rohde, G. Thalhammer, J. Eschner, F. Schmidt-Kaler, and R. Blatt, Laser addressing of individual ions in a linear ion trap, *Phys. Rev. A* **60**, 145 (1999).
- [27] C. Piltz, T. Sriarunothai, A. Varón, and C. Wunderlich, A trapped-ion-based quantum byte with 10^{-5} next-neighbour cross-talk, *Nat. Commun.* **5**, 4679 (2014).
- [28] U. Warring, C. Ospelkaus, Y. Colombe, R. Jördens, D. Leibfried, and D. J. Wineland, Individual-ion addressing with microwave field gradients, *Phys. Rev. Lett.* **110**, 173002 (2013).
- [29] J. Randall, S. Weidt, E. D. Standing, K. Lake, S. C. Webster, D. F. Murgia, T. Navickas, K. Roth, and W. K. Hensinger, Efficient preparation and detection of microwave dressed-state qubits and qutrits with trapped ions, *Phys. Rev. A* **91**, 012322 (2015).
- [30] D. P. L. Aude Craik, N. M. Linke, M. A. Sepiol, T. P. Harty, J. F. Goodwin, C. J. Ballance, D. N. Stacey, A. M. Steane, D. M. Lucas, and D. T. C. Allcock, High-fidelity spatial and polarization addressing of $^{43}\text{Ca}^+$ qubits using near-field microwave control, *Phys. Rev. A* **95**, 022337 (2017).
- [31] R. Sutherland, R. Srinivas, and D. Allcock, Individual addressing of trapped ion qubits with geometric phase gates, *Phys. Rev. A* **107**, 032604 (2023).
- [32] R. Srinivas, C. M. Löschnauer, M. Malinowski, A. C. Hughes, R. Nourshargh, V. Negnevitsky, D. T. C. Allcock, S. A. King, C. Matthesen, T. P. Harty, and C. J. Ballance, Coherent control of trapped ion qubits with localized electric fields, *Phys. Rev. Lett.* **131**, 020601 (2023).
- [33] A. D. Leu, M. F. Gely, M. A. Weber, M. C. Smith, D. P. Nadlinger, and D. M. Lucas, Fast, high-fidelity addressed single-qubit gates using efficient composite pulse sequences, *Phys. Rev. Lett.* **131**, 120601 (2023).
- [34] A. Khromova, C. Piltz, B. Scharfenberger, T. F. Gloer, M. Johanning, A. F. Varón, and C. Wunderlich, Designer spin pseudomolecule implemented with trapped ions in a magnetic gradient, *Phys. Rev. Lett.* **108**, 220502 (2012).
- [35] A. Sørensen and K. Mølmer, Entanglement and quantum computation with ions in thermal motion, *Phys. Rev. A* **62**, 022311 (2000).
- [36] A. Sørensen and K. Mølmer, Quantum computation with ions in thermal motion, *Phys. Rev. Lett.* **82**, 1971 (1999).
- [37] G. Milburn, S. Schneider, and D. James, Ion trap quantum computing with warm ions, *Fortschr. Phys.* **48**, 801 (2000).
- [38] M. A. Weber, C. Löschnauer, J. Wolf, M. F. Gely, R. K. Hanley, J. F. Goodwin, C. J. Ballance, T. P. Harty, and D. M. Lucas, Cryogenic ion trap system for high-fidelity near-field microwave-driven quantum logic, *Quantum Sci. Technol.* **9**, 015007 (2024).
- [39] See Supplemental Material at <http://link.aps.org/supplemental/10.1103/PRXQuantum.5.030321> for more information including: (1) derivation of the Hamiltonian, (2) measurements and modelling of the microwave field, (3) calibrations performed when displacing the ion, (4) the choice of parameters for the microwave pulses used in this work, (5) further details of the simulations presented in Fig. 5, and (6) further details of the measurements shown in Fig. 6.
- [40] C. Monroe, D. M. Meekhof, B. E. King, and D. J. Wineland, A “Schrödinger cat” superposition state of an atom, *Science* **272**, 1131 (1996).
- [41] A. H. Myerson, D. J. Szwer, S. C. Webster, D. T. C. Allcock, M. J. Curtis, G. Imreh, J. A. Sherman, D. N. Stacey, A. M. Steane, and D. M. Lucas, High-fidelity readout of trapped-ion qubits, *Phys. Rev. Lett.* **100**, 200502 (2008).
- [42] D. Hayes, S. M. Clark, S. Debnath, D. Hucul, I. V. Inlek, K. W. Lee, Q. Quraishi, and C. Monroe, Coherent error suppression in multiqubit entangling gates, *Phys. Rev. Lett.* **109**, 020503 (2012).
- [43] M. G. House, Analytic model for electrostatic fields in surface-electrode ion traps, *Phys. Rev. A* **78**, 033402 (2008).
- [44] H. Hahn, G. Zarantonello, A. Bautista-Salvador, M. Wahnschaffe, M. Kohnen, J. Schoebel, P. O. Schmidt, and C. Ospelkaus, Multilayer ion trap with three-dimensional microwave circuitry for scalable quantum logic applications, *Appl. Phys. B* **125**, 154 (2019).
- [45] D. P. L. Aude Craik, N. M. Linke, T. P. Harty, C. J. Ballance, D. M. Lucas, A. M. Steane, and D. T. C. Allcock, Microwave control electrodes for scalable, parallel, single-qubit operations in a surface-electrode ion trap, *Appl. Phys. B* **114**, 3 (2014).
- [46] U. Warring, C. Ospelkaus, Y. Colombe, K. R. Brown, J. M. Amini, M. Carsjens, D. Leibfried, and D. J. Wineland, Techniques for microwave near-field quantum control of trapped ions, *Phys. Rev. A* **87**, 013437 (2013).
- [47] M. Brownnutt, M. Kumph, P. Rabl, and R. Blatt, Ion-trap measurements of electric-field noise near surfaces, *Rev. Mod. Phys.* **87**, 1419 (2015).
- [48] G. D. Vittorini, *Stability of ion chains in a cryogenic surface-electrode ion trap*, Ph.D. thesis, Georgia Tech, 2013, Sec. 4.2.
- [49] S.-L. Zhu, C. Monroe, and L.-M. Duan, Arbitrary-speed quantum gates within large ion crystals through minimum control of laser beams, *Europhys. Lett.* **73**, 485 (2006).
- [50] T. Choi, S. Debnath, T. A. Manning, C. Figgatt, Z.-X. Gong, L.-M. Duan, and C. Monroe, Optimal quantum control of multimode couplings between trapped ion qubits for scalable entanglement, *Phys. Rev. Lett.* **112**, 190502 (2014).
- [51] F. Kranzl, M. K. Joshi, C. Maier, T. Brydges, J. Franke, R. Blatt, and C. F. Roos, Controlling long ion strings for quantum simulation and precision measurements, *Phys. Rev. A* **105**, 052426 (2022).
- [52] E. Knill, D. Leibfried, R. Reichle, J. Britton, R. B. Blakestad, J. D. Jost, C. Langer, R. Ozeri, S. Seidelin, and D. J. Wineland, Randomized benchmarking of quantum gates, *Phys. Rev. A* **77**, 012307 (2008).

- [53] M. Cetina, L. Egan, C. Noel, M. Goldman, D. Biswas, A. Risinger, D. Zhu, and C. Monroe, Control of transverse motion for quantum gates on individually addressed atomic qubits, [PRX Quantum 3, 010334 \(2022\)](#).
- [54] K. A. Landsman, Y. Wu, P. H. Leung, D. Zhu, N. M. Linke, K. R. Brown, L. Duan, and C. Monroe, Two-qubit entangling gates within arbitrarily long chains of trapped ions, [Phys. Rev. A 100, 022332 \(2019\)](#).
- [55] D. Kielpinski, C. Monroe, and D. J. Wineland, Architecture for a large-scale ion-trap quantum computer, [Nature 417, 709 \(2002\)](#).
- [56] C. Monroe, R. Raussendorf, A. Ruthven, K. R. Brown, P. Maunz, L.-M. Duan, and J. Kim, Large-scale modular quantum-computer architecture with atomic memory and photonic interconnects, [Phys. Rev. A 89, 022317 \(2014\)](#).